AIHA Journal

ISSN: 1542-8117 (Print) (Online) Journal homepage: https://www.tandfonline.com/loi/uaih20

Comparison of Emission Models With Computational Fluid Dynamic Simulation and a Proposed Improved Model

James S. Bennett , Charles E. Feigley , Jamil Khan & Mohammad H. Hosni

To cite this article: James S. Bennett , Charles E. Feigley , Jamil Khan & Mohammad H. Hosni (2003) Comparison of Emission Models With Computational Fluid Dynamic Simulation and a Proposed Improved Model, AIHA Journal, 64:6, 739-754, DOI: 10.1080/15428110308984868

To link to this article: https://doi.org/10.1080/15428110308984868

Published online: 04 Jun 2010.

AIHA Journal 64:739–754 (2003) Ms. #457

Comparison of Emission Models With Computational Fluid Dynamic Simulation and a Proposed Improved Model

AUTHORS
James S. Bennett[a]
Charles E. Feigley[b]
Jamil Khan[c]
Mohammad H. Hosni[d]

[a]Centers for Disease Control and Prevention, National Institute for Occupational Safety and Health, Division of Applied Research and Technology, Engineering and Physical Hazards Branch, 4676 Columbia Parkway MS-R5, Cincinnati, OH 45226;
[b]Department of Environmental Health Sciences, University of South Carolina, Columbia, S.C.;
[c]Department of Mechanical Engineering, University of South Carolina, Columbia, S.C.;
[d]Department of Mechanical and Nuclear Engineering, College of Engineering, Kansas State University, Manhattan, KS 66506

Understanding source behavior is important in controlling exposure to airborne contaminants. Industrial hygienists are often asked to infer emission information from room concentration data. This is not easily done, but models that make simplifying assumptions regarding contaminant transport are frequently used. The errors resulting from these assumptions are not yet well understood. This study compares emission estimates from the single-zone completely mixed (CM-1), two-zone completely mixed (CM-2), and uniform diffusivity (UD) models with the emissions set as boundary conditions in computational fluid dynamic (CFD) simulations of a workplace. The room airflow and concentration fields were computed using Fluent 4. These numerical experiments were factorial combinations of three source locations, five receptor locations, three dilution airflow rates, and two generation rate profiles, constant and time-varying. The aim was to compute plausible concentration fields, not to simulate exactly the processes in a real workroom. Thus, *error* is defined here as the difference between model and CFD predictions. For the steady-state case the UD model had the lowest error. When the source near-field contained the breathing zone receptor, the CM-2 model was applied. Then, in decreasing agreement with CFD were UD, CM-2, and CM-1. Averaging over all source and receptor locations (CM-2 applied for only one), in decreasing order of agreement with CFD were UD, CM-1, and CM-2. Source and receptor location had large effects on emission estimates using the CM-1 model and some effect using the UD model. A location-specific mixing factor (location factor) derived from steady-state concentration gradients was used to build a more accurate time-dependent emission model, CM-L. Total mass emitted from a time-varying source was modeled most accurately by CM-L, followed by CM-1 and CM-2.

Keywords: airborne contaminants, computation fluid dynamics, emission models

Advances in computing capability now allow numerical modeling to perform a greater portion of the work in many technical fields, including occupational health. Even simple models generally are implemented on a computer, and the availability of inexpensive, user-friendly computing power has led to increasing application of mathematical models by industrial hygienists. Models may be empirical, deterministic, or contain elements of both. Although empirical models are built on real data, their application may be limited to the specific situation in which the data were collected. Simple deterministic models can be applied in a variety of situations, but the fit to any single scenario depends on the model assumptions. A deterministic model can be no better than the scientific laws from which it is built. The physics of simple mass balance models is sound, when their assumptions are valid, but the transport processes in occupational environments are more complicated than these models assume.

Accuracy of simple, deterministic mass-balance models for estimating emissions has only

begun to be systematically investigated for realistic scenarios, although their performance in idealized, hypothetical situations has been assessed.[1] Comparison with experimental measurements of spatial and temporal concentration distribution is one means to evaluate models. An alternative method of generating a concentration field, C(x,y,z,t), is computational fluid dynamics (CFD), the numerical solution of the fundamental equations that describe fluid behavior, here applied to the transport of a gas-phase contaminant in air. CFD is itself a deterministic model, mainly. However, a good CFD model, which typically contains some empirical features, captures the relevant physics[2] of contaminant transport, generating plausible concentration fields that provide meaningful comparisons to simple deterministic models. As other researchers continue to demonstrate good agreement between measured concentration fields and fields simulated using CFD,[3,4] the potential of CFD as a means of simple model evaluation becomes evident. The effectiveness of this approach stems from the relative ease with which variables such as room shape and supply air inlet velocity can be changed and detailed spatial concentration information obtained.

Three (deterministic) mass balance models have been widely applied: the one-zone completely mixed model, the two-zone completely mixed model, and the uniform hemispherical diffusion model.[1,5–13] For convenience these will be referred to as CM-1, CM-2, and UD, respectively. A fourth mass-balance model is proposed here, CM-L, that combines workable ideas from CM-1 and CM-2.

The models are applied here to an embalming room that has been the subject of earlier studies by Stewart et al.[14] and Bennett et al.[5,6] Plausible concentration fields are resolved by using CFD to simulate the room airflow in realistic conditions. This work is meant to show how the emission predictions of CM-1, CM-2, CM-L, and UD compare with the emission information used in the CFD simulations. It will be demonstrated that the performance of these models depends on the conditions in which they are applied.

METHODS

CFD

Software and User Interface

The numerical simulations were performed using the commercial CFD software, Fluent 4 (Fluent, Inc., Lebanon, N.H.). The geometry setup, grid formation, numerical solution, and graphical display of results were handled by Fluent 4 without using separate geometry/grid formation or solution display/manipulation software.

Geometry and Grid Formation

The three-dimensional room simulation, including the worker and objects, was constructed using a uniform grid of 10,400 rectangular cells, 16.6 × 17.1 × 15.4 cm. Figure 1 is a plan view of the actual room, showing monitoring and source locations. "CEA Inlet" refers to the intake location of the TGM-555 toxic gas monitor (CEA Instruments, Emerson, N.J.) that sampled formaldehyde at 1-sec intervals in the study by Stewart et al.[14] The "monitoring" locations in the simulation corresponded to those in Stewart et al., except that the embalmer's breathing zone here was assumed to be stationary to characterize a very frequent embalmer location in the room. The exhaust concentration estimated by CFD also was considered in this analysis. The area station 1 (A1), area station 2 (A2), and CEA locations were at a height of 1.97 m, breathing zone (BZ) at 1.46 m, and exhaust at 0.257 m. Three source locations were chosen for the placement of contaminant inlet cells, "floor," "pump," and "table." These were based on Stewart et al.'s observations that embalming fluid spills, mixing/preparation of embalming fluids, and application of formaldehyde-containing products to the thoracic and abdominal cavities were followed by increases in room formaldehyde concentrations. The black squares shown in Figures 2 through 4 indicate the source locations. Heights for the floor, pump, and table sources were 0.000, 1.20, and 1.03 m.

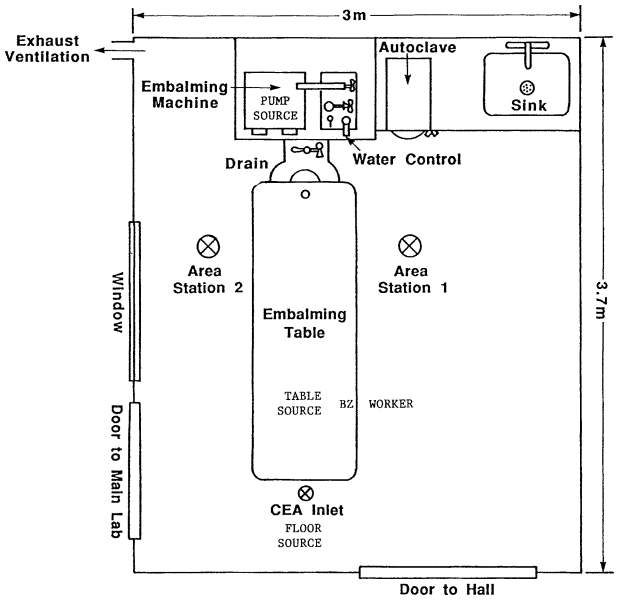

FIGURE 1. Plan view of the actual room, showing monitoring and source locations

Numerical Solution

Fluent 4 uses the control volume method.[15] The basic computational element is a small volume or cell. Whereas the Navier-Stokes equations (fundamental conservation equations that describe fluid motion) apply to a fluid continuum, the control

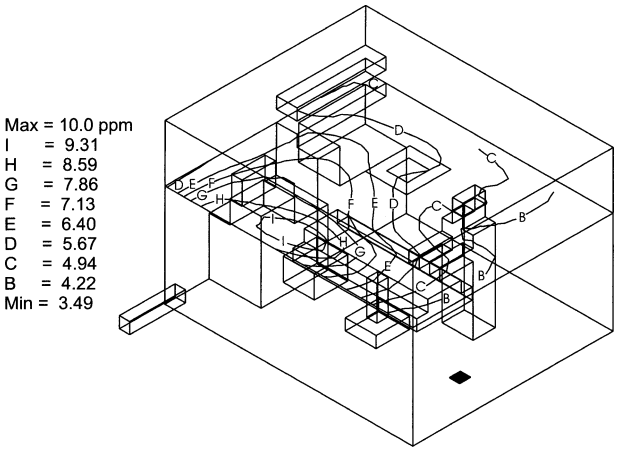

FIGURE 2. Simulated formaldehyde concentration field in units of parts per million at BZ height for the floor source location (indicated by the black square), at the moderate ventilation rate

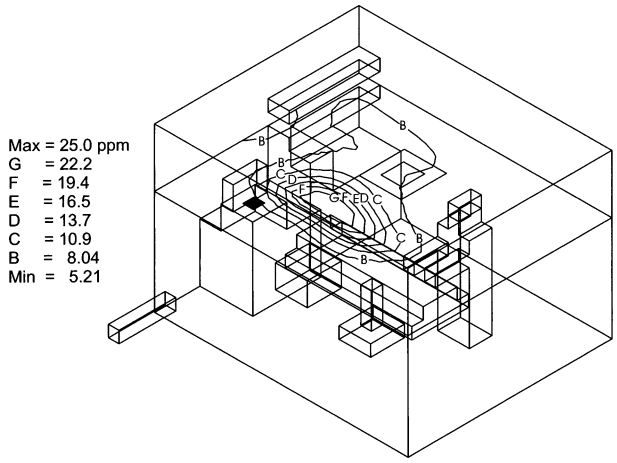

FIGURE 3. Simulated formaldehyde concentration field in units of parts per million at BZ height for the pump source location (indicated by the black square), at the moderate ventilation rate

volume method adapts these equations to a set of grid points. These disctretized equations are written for each cell in terms of the neighboring cells.[16] Using ϕ as a general variable to represent mass, momentum, or energy, the continuum form of the general conservation equation in Cartesian coordinates is, [16,17]

$$\frac{\partial}{\partial t}(\rho\phi) + \frac{\partial}{\partial x}(\rho u\phi) + \frac{\partial}{\partial y}(\rho v\phi) + \frac{\partial}{\partial z}(\rho w\phi) = \frac{\partial}{\partial x}\left(\Gamma_\phi \frac{\partial \phi}{\partial x}\right) + \frac{\partial}{\partial y}\left(\Gamma_\phi \frac{\partial \phi}{\partial y}\right) + \frac{\partial}{\partial z}\left(\Gamma_\phi \frac{\partial \phi}{\partial z}\right) + S_\phi. \quad (1)$$

When this partial differential equation is discretized in the control volume method, it becomes,

$$\phi_P \sum_i (A_i - S_P) = \sum_i (A_i \phi_i) + S_C \quad (2)$$

where i = N, S, E, W, F, B (or north, south, east, west, front, back), relative to the grid point P.[18] The A's are convective and diffusive flux coefficients between cells, and S_C and S_P are the components of the linearized source term, $S_\phi = S_C + S_P\phi$.[16,18]

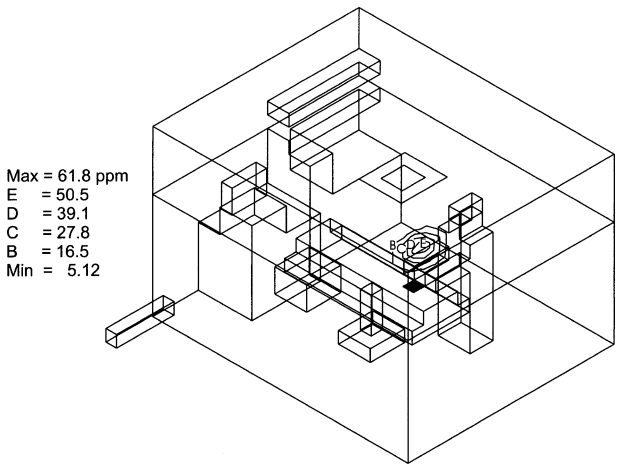

FIGURE 4. Simulated formaldehyde concentration field in units of parts per million at BZ height for the table source location (indicated by the black square), at the moderate ventilation rate

The starting point for the calculation is an explicit value (provided by the user) of the solution variables at a boundary of the computational domain, for example, the air velocity and turbulence parameters over the face of a ceiling diffuser. Initially, the gauge pressure was set to zero in each cell.

The solution proceeded through the following steps.

(1) Solve Equation 2 for each velocity component by substituting that component for ϕ, using the current pressure field. These are the conservation of momentum equations that update the velocity components.

(2) Solve a "pressure correction" equation to adjust the pressure and velocity fields so that conservation of mass is achieved locally.

(3) Solve Equation 2 for the kinetic energy of turbulence, k, and the eddy dissipation rate, ϵ, using the new velocity field.

(4) Check the solution for convergence. If yes, stop. If no, repeat the process, starting at step 1.

This process is the SIMPLE algorithm of Patankar and Spalding.[17–19] The converged solution for the flow field was then used as the starting point for the contaminant concentration calculation. The user provided the contaminant mole fraction at the ceiling diffuser (zero) and the contaminant source inlet (0.5 for the steady-state simulation; the true generation rate function in Figure 5 converted to mole fraction for the time-dependent simulation). The SIMPLE algorithm was applied again. However, two new steps were added between steps 3 and 4: (1) Solve the contaminant conservation equation and update the concentration field, and (2) update the density and viscosity of the fluid, based on the concentration.

Separating the clean flow field and contaminant calculations in this way allowed a steady-state, clean airflow simulation to be used as the starting point for the time-dependent contaminant source calculation, for computational efficiency.

Physical Modeling: Turbulence and Chemistry

Turbulence was handled through the k-ϵ model, with standard wall functions.[20,21] The empirical constants for the model were set at their standard values, which are the default settings in the commercial CFD code. The grid spacing in the boundary layer near the room walls and the other surfaces was consistent with the assumptions of the standard wall functions. Because the simulations were performed under isothermal conditions, buoyancy was not included in the turbulence model. A description of this turbulence model is provided in the Appendix.

The contaminated room air was modeled as a two-component mixture of air and formaldehyde. Concentration was treated as a volume fraction. The average temperature of the room air during the embalming experiments (72.7°F) and the molecular weights of formaldehyde and air were used with the gas law to compute the density. The mixture density was computed by the CFD code as a field function that depended on the concentration at each cell location. The fluid viscosity was assumed to be constant and was set at the viscosity of air at the average temperature during the embalming experiments.

Boundary Conditions

The airflow distribution from the ceiling diffuser was characterized experimentally. These results were then used as CFD boundary conditions, like the methods developed by Nielsen.[22,23] A preliminary investigation determined that inlet flow distribution has a crucial influence on the flow in the room as a whole. Zhang et al.

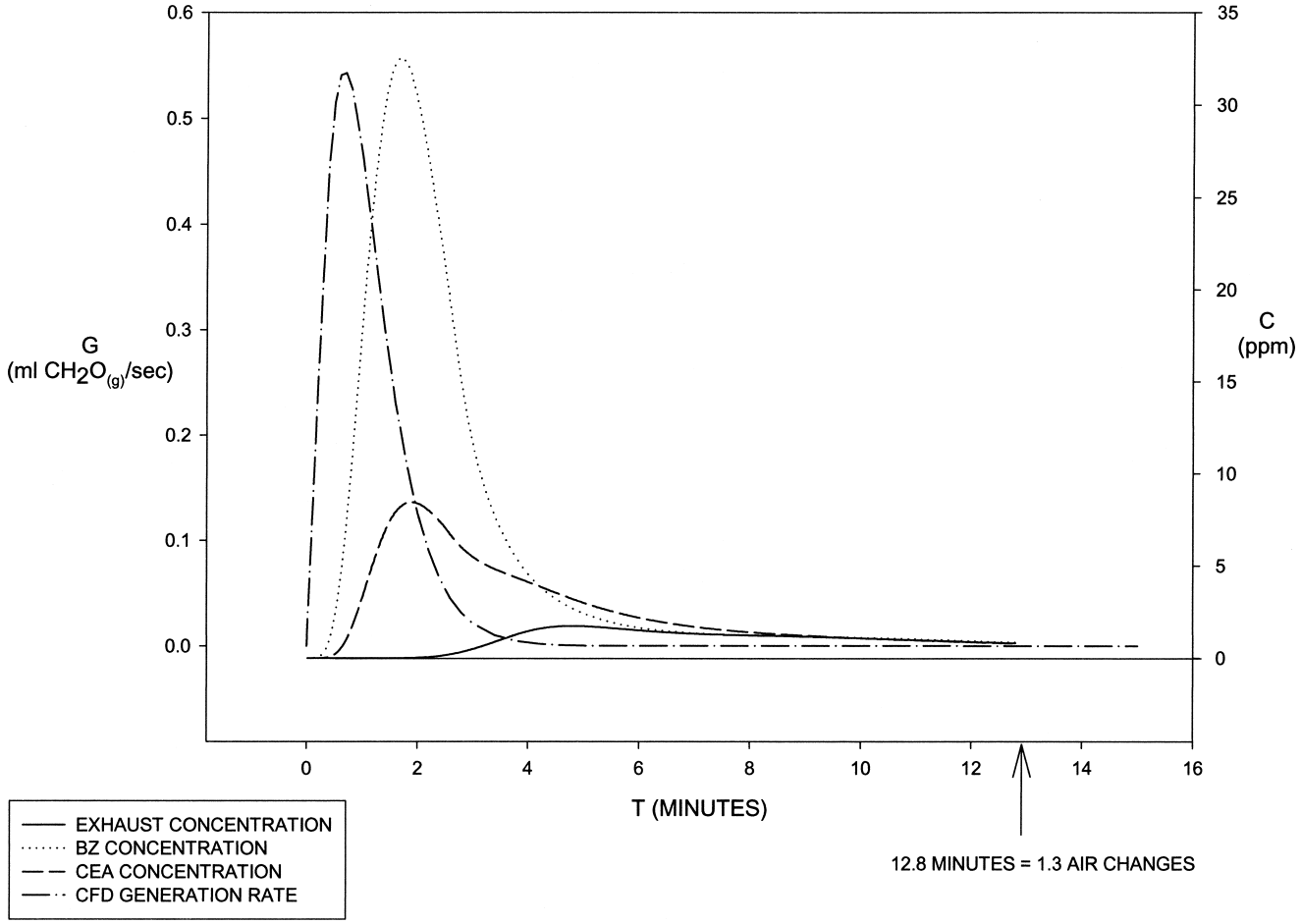

FIGURE 5. True generation rate function and simulated concentration at the BZ, CEA, and exhaust locations

also reports this influence.[24] To that end the supply portion of the ventilation system was reproduced in the laboratory. Velocity measurements at 24 points near the diffuser were used as boundary conditions in the simulation. These measurements are found in Bennett.[25] A fan drove flow through the same diameter and type of flexible duct and out of the same type and size of ceiling diffuser. Importantly, the lengths and angles of the ductwork were reproduced, so that the loading of the diffuser was replicated. However, the relative loading was kept constant across the three ventilation rates in the simulation, with the velocity profile scaled to fit the ventilation rates. Turbulence quantities were also specified. The turbulence intensity was assumed to be 10% at the inlet, and the turbulence length scale was set at 3.81 cm, the separation between vanes of the diffuser, using the idea that an eddy can be no larger than the flow boundary allows.[26] Because turbulence is generated and dissipated by flows, its specification at flow boundaries is less important than the specification of a conserved quantity, such as mass flow rate. Therefore, some arbitrariness in the turbulence boundary condition is acceptable. The simulations were performed under isothermal conditions.

Simulations were performed for both constant and time-varying emission rates, yielding steady-state and time-dependent solutions. For the steady-state case a nominal contaminant generation rate was arbitrarily chosen, because only relative concentration affects model performance. In the time-dependent case an estimated generation rate function from earlier work was adopted.[5] This generation rate function, shown in Figure 5, corresponded to a work task that contributes highly to formaldehyde exposure during embalming, the application of osmotic gel. As with the steady-state rate, the selection of the time-dependent rate function was somewhat arbitrary and serves only as an example of the effect of a time-dependent concentration field on model prediction. The shape of the function affects model performance, making the time-dependent portion of this analysis more applicable to generation rate functions of this form.

Verification and Validation

The authenticity of CFD solutions can be decomposed into two areas, verification and validation.[27] The American Institute of Aeronautics and Astronautics defines verification as "the process of determining that a model implementation accurately represents the developer's conceptual description of the model and the solution to the model." Validation is defined as "the process of determining the degree to which a model is an accurate representation of the real world from the perspective of the intended uses of the model."[27, pp. 11–15] The following are the specific verification tests that were performed, along with their outcomes.

Code Implementation. Fluent 4 is a commercial code that has been widely used in academia, government, and industry for many years. The authors accepted that the code was without major programming defects.

Spatial Discretization (Grid Convergence). The results from the

original grid were compared with a new grid in which the number of cells in the room volume was doubled in each direction (the number of cells in the room volume increased by a factor of eight). Cell dimensions of the new grid were 8.28 × 8.59 × 7.72 cm. The absolute value of the percentage difference in steady-state concentrations over all combinations of source location, receptor location, and ventilation rate had a median value of 4.24%. The differences ranged from −58 to 25%.

Temporal Discretization. The concentration as a function of time at the five receptor locations for both the original time step of 0.5 sec and the reduced time step, 0.25 sec, were compared and found to be indistinguishable. This showed that the numerical solution was not improved by a shorter time step.

Solution Convergence. The solution process was iterated until the sum of the normalized residuals for each conservation equation was less than 10^{-5}.

The following specific validation tests were performed, along with their outcomes.

Physical Plausibility. For the steady-state cases the CFD exhaust concentration was compared with G_{bc}/Q_{bc}, where G_{bc} and Q_{bc} were the boundary conditions used in the simulation. In the time-dependent case the CFD emission estimate taken in the exhaust was compared with the time integral of G_{bc}. The simulated and theoretical results were identical at three significant figures.

Experimental Measurements. To independently validate the CFD simulations, experimental results for a full-sized test room described by Hosni et al. were compared with numerical simulations for that room, using CFD methods identical to the present study.[28] In the present study the empty room Reynolds number ranged from 157 to 2050, whereas it was 2400 for the test room used in the previous validation study. The experimental results included airspeed measurements using both an omnidirectional probe and a three-dimensional hot film probe throughout the vertical center-plane that included the supply and return inlets. The experimental results showed that the velocity varied greatly from the supply jet region to the occupied region of the room. Because the accuracy of velocity measurements using the three-dimensional probe is limited to air velocities above 0.15 m/sec and requires the probe to be positioned within the 70° cone angle, it was decided to use the airspeed instead of velocity for validation tests in the occupied region of the room. Furthermore, in the jet region the axial velocity component has approximately the same magnitude as the airspeed. Because the jet core direction was known and the jet plays a major role in the general room airflow distribution, airspeed was a logical choice for validation. The CFD simulation and the experimental results differed by less than 30% in all regions of the room along the center-plane where a contaminant source or receptor might be located and differed negligibly at a standing BZ of 1.5 m.

Returning to the present study, the supply air boundary condition inputs for the CFD code were based on measured velocities at the ceiling diffuser, as explained earlier. Implementation of boundary conditions is also an aspect of validation.

Limitations and Intended Use

Simulation of airflow and contaminant transport in occupied spaces is at the forefront of CFD research. To capture these behaviors with a high degree of accuracy usually requires grid and time step refinement that can directly simulate the larger eddies.[29] This was certainly not achieved here, as the simulation used a coarse grid and a Reynolds-averaged Navier-Stokes (RANS) turbulence model, described in the Appendix. It is also important to recognize that tests of validation are not fully independent of one another.[30] For example, the temporal discretization test yielded essentially no difference between a time step of 0.5 and 0.25 sec. However, if the grid had been fine enough to resolve the structure of eddies, the temporal discretization test might have failed at 0.5 sec. Rather than attempt a highly accurate simulation of this particular room and set of conditions, the authors sought to formulate plausible concentration fields that are accurate enough to provide informative bases of comparison with CM-1, CM-2, and UD. This approach was also limited by the isothermal assumption and the stationary worker. Moreover, even a perfect characterization of a limited set of room geometries and operating conditions should not be used to make statements about model accuracy in all conditions.

Simple Deterministic Models

CM-1

Assuming that the dilution air is clean and, for the time-dependent case, that the room is initially clean, the CM-1 model is represented by the following equations.[9]

$$\text{Steady-state} \qquad G = QC \tag{3}$$

$$\text{Time-dependent} \qquad G = V\frac{dC}{dt} + QC. \tag{4}$$

G, C, Q, and V are the contaminant generation rate, concentration, dilution ventilation flow rate, and room volume, respectively.

To implement CM-1 for the simulations, the dilution ventilation rate, Q_{bc}, and contaminant generation rate, G_{bc}, were specified as CFD boundary conditions, with Q_{bc} also used as an input parameter for CM-1. In evaluating the steady-state model, the simulated concentration at a sampling location, C_{cfd}, was entered in Equation 3 to find G predicted by the model, G_m:

$$G_m = Q_{bc}C_{cfd} \tag{5}$$

Next, the error was found by comparing G_m with G_{bc}:

$$\text{error} = \left(\frac{G_m - G_{bc}}{G_{bc}}\right)100\%. \tag{6}$$

Model evaluation for the time-dependent source involved numerical approximation of the derivative of concentration with respect to time.[31] Next, $G_m(t)$, formed from the simulated concentration, was integrated numerically using Simpson's rule[32] to find the total mass of contaminant emitted, $_m$.

$$\gamma_m = \int_0^\infty G_m\,dt = \int_0^\infty \left(V\frac{dC_{cfd}}{dt} + Q_{bc}C_{cfd}\right)dt. \tag{7}$$

A finite integration limit of 1.30 air changes was chosen to actually do this calculation. This corresponded to 60.0, 12.8, and 5.03 min for the low, moderate, and high ventilation rates, respectively. Although purging of the room was incomplete after this amount of time, it seemed more reasonable to truncate the integration to a period that was of the same time scale as many of the work tasks observed in Stewart et al.'s study[14] than to extend the integration until the concentrations had decayed to essentially zero. For example, 4.61 air changes are required for a completely mixed space with no sources or sinks to decay to 1% of the initial concentration. For the low ventilation rate this would have required 212 min, which would be impractical when an attempt is being made to characterize a series of emissions discretely. The truncation challenged CM-1, because the integrals included little of the completely mixed period.

Slightly different than before, the error was found by comparing γ_m with $\gamma_{bc,}$ which was the total mass generated in the simulation through the boundary condition, $G_{bc}(t)$.

$$\text{error} = \left(\frac{\gamma_m - \gamma_{bc}}{\gamma_{bc}}\right)100\%. \quad (8)$$

Also, $G_m(t)$ was compared graphically with $G_{bc}(t)$ to determine whether the instantaneous behavior was modeled accurately.

Returning to the steady-state case, it was shown by Bennett et al. that the simulated concentration at a specific location was linearly related to (G/Q).[6] This was true for each source location. Regression analysis gave an R^2 greater than 0.998. In other words, the error in the CM-1 model applied to concentration estimation at a specific source and receptor location pair was nearly constant across ventilation rate, for the range 0.522 to 6.23 m^3/min. The location-specific error in the CM-1 model was defined as a location factor, λ_i, where:

$$\lambda_i = \frac{C_i}{(G/Q)}. \quad (9)$$

The λ_i were the slopes of the linear relationships between the C_i and (G/Q). In the present study the error in steady-state emission estimation can also be expressed in terms of the location factor by combining Equations 6 and 9:

$$\text{error} = \frac{G_m - G_{cfd}}{G_{cfd}} = \frac{QC_i - G_{cfd}}{G_{cfd}} = \frac{C_i - (G_{cfd}/Q)}{G_{cfd}/Q}$$

$$= \frac{C_i}{G_{cfd}/Q} - 1 = \lambda_i - 1. \quad (10)$$

Also, multiplying both sides of Equation 9 by G yields Equation 11, in which the product of the location factor and the true generation rate defines the apparent generation rate:

$$G_{AP} = \lambda_i G = C_i Q \quad (11)$$

Applying Equation 3 to the concentration measured at location i results in the apparent generation rate instead of the true generation rate. If the CM assumption is true, the location factor is unity everywhere in the space, the apparent generation rate is the true generation rate, and the error is zero.

CM-2

In the two-zone model (CM-2) used by Nicas, mass balances are applied to a zone that includes the contaminant source and to another zone that includes the remainder of the room volume.[8] These zones are termed near-field and far-field, respectively. Relations like Equations 3 and 4 are written for both zones with an interzone air exchange rate, β:

$$\frac{dC_N}{dt} = -\frac{\beta}{V_N}C_N(t) + \frac{\beta}{V_N}C_F(t) + \frac{G}{V_N} \quad (12)$$

$$\frac{dC_F}{dt} = \frac{\beta}{V_F}C_N(t) + \frac{-(Q+\beta)}{V_F}C_F(t) \quad (13)$$

$$\frac{dG}{dt} = 0. \quad (14)$$

Equation 4 simply indicates that the emission rate is constant. The system of differential equations can be solved to yield the concentrations. If the emission rate is constant for a sufficiently long time, a steady-state is reached. Then, concentration and emission are related as follows:

$$G = \frac{\beta Q C_N}{\beta + Q} \quad (15)$$

$$G = QC_F. \quad (16)$$

β can be determined experimentally through velocity measurements and the projected area of the near-field zone.[6] It can also be found from the mass balance equations. For example, Equation 15 can be solved for β if the near-field zone concentration, generation rate, and ventilation rate, Q, are known. In this work β was calculated from the CFD-generated steady-state velocity field U(x,y,z) at the boundary between the near and far field zones. Complete mixing is assumed within each zone, with a concentration discontinuity at the zonal boundary.

A model that restricts the emission rate to being constant can be used for the transient behavior following a step change in the emission rate of an otherwise constant source. The present authors were interested in the fully time-dependent case, in which both emission rate and concentration were functions of time. Thus, Equation 2 was rearranged to:

$$G = V_N\frac{dC_N}{dt} + \beta(C_N - C_F). \quad (17)$$

Another option is to add Equations 2 and 3, resulting in an expression that does not require β:

$$G = V_N\frac{dC_N}{dt} + V_F\frac{dC_F}{dt} + QC_F. \quad (18)$$

As before, Equation 6 was used to calculate the error in the steady-state case and Equation 8 in the time-dependent case. $G_m(t)$ and $G_{bc}(t)$ were also compared graphically.

CM-L

Here the authors propose a modified CM model, for time-varying emission rates, derived by applying the conservation of mass principle to a conceptual sphere within a room. The sphere is centered at the point source and has a radius equal to the distance between the source and a receptor. Within the volume of the sphere, V_i:

$$\text{accumulation rate} = \text{generation rate} - \text{removal rate}. \quad (19)$$

The assumption is made that the concentration, C(t), is spatially uniform within V_i and on its boundary. Receptor location i is on the sphere boundary. Therefore:

$$C(t) = C_i(t) \quad (20)$$

It follows that:

$$\frac{dC}{dt} = \frac{dC_i}{dt}. \quad (21)$$

Then, the accumulation rate becomes:

$$\iiint_{V_i}\frac{dC}{dt}\,dV = \frac{dC_i}{dt}\iiint_{V_i}dV = V_i\frac{dC_i}{dt}. \quad (22)$$

To derive the removal rate, assume for a moment that a steady-state has been reached, so that the accumulation rate is zero. Then, inspection of Equation 9 shows that the removal rate and the generation rate, G, are equal. Equation 9 applies to any volume that contains the source, including the room itself. Because the removal rates from the sphere and from the room are each equal to G, they must also be equal to each other. An expression for the removal rate from the room, then, can be used as the removal rate from the sphere. Assuming there are no sinks, so that

removal from the room is due only to exhaust flow, Q, then the removal rate from the room or the sphere is the product QC_{ex}; and,

$$QC_{ex} = G, \tag{23}$$

where C_{ex} is the room exhaust concentration. Dividing both sides by Q:

$$C_{ex} = \frac{G}{Q}. \tag{24}$$

Using Equation 9, which defines the location factor, λ, in terms of G/Q, the removal rate from the sphere volume, V_i, can be written as:

$$QC_{ex} = \frac{1}{\lambda_i} QC_i. \tag{25}$$

λ_i was calculated through a steady-state simulation that provided C_i, using G and Q as boundary conditions. The equivalent experimental procedure would have been to measure C_i resulting from a source with constant emission rate, in a room under general ventilation rate, Q.

The assumption is made that Equation 25, derived for the steady-state, is approximately true also for a weakly time-dependent source. This assumption is reasonable only when the generation rate changes slowly compared with the residence time, because a quasi steady-state is maintained. Then with generation rate, G(t), Equation 19 becomes:

$$V_i \frac{dC_i}{dt} = G(t) - \frac{1}{\lambda_i} QC_i, \quad \text{or,} \tag{26}$$

$$G(t) = V_i \frac{dC_i}{dt} + \frac{1}{\lambda_i} QC_i. \tag{27}$$

When the emission rate changes rapidly, the removal rate is not accurately characterized. However, the consequences of this inaccuracy are lessened by the dominance of the accumulation rate in such a situation. Consider Equation 27 after time-dependence has been recast as frequency-dependence by applying the Laplace transform to both sides:

$$\mathbf{G}(s) = L\{G(t)\} = L\left\{V_i \frac{dC_i}{dt} + \frac{1}{\lambda_i} QC_i\right\}. \tag{28}$$

Using the linearity and differentiation properties of the Laplace transform,[33]

$$\mathbf{G}(s) = V_i s \mathbf{C}_i(s) + \frac{1}{\lambda_i} Q \mathbf{C}_i(s) = \mathbf{C}_i(s)\left[V_i s + \frac{1}{\lambda_i} Q\right]. \tag{29}$$

As the frequency, s, becomes large, which is equivalent to the generation rate changing rapidly, the right-hand side of Equation 29 approaches $C_i(s)[V_i s]$:

$$G(s) \approx C_i(s)[V_i s]. \tag{30}$$

Applying the inverse Laplace transform to go back to time-dependence results in an expression that does not involve the removal rate:

$$G(t) \approx V_i \frac{dC_i}{dt}. \tag{31}$$

Thus, although Equation 27 is certainly not strictly true, its error is lessened, by being a reasonable approximation both for very slowly and very rapidly changing generation rates.

In applying this model to the simulated room, there were situations in which portions of the sphere boundary extended beyond the room. The researchers proceeded anyway, thinking of a volume quantity, V_i, with a shape that might be a sphere flattened and widened on one side for example. This was loosely based on how flows spread out when incident on a wall, due to vortex squeezing[34] and flow along the wall, because of conservation of momentum. The upper limit of V_i was set equal to the room volume, V.

UD

Many investigators have applied a model, here called the UD model, that assumes a contaminant is transported from the source by isotropic turbulence.[10–13] They obtained eddy diffusivity, D, measurements for use in the hemispherical mass balance equation for isotropic diffusion,

$$G = \frac{2\pi r D C}{1 - \text{erf}\left(\frac{r}{\sqrt{4Dt}}\right)}. \tag{32}$$

The steady-state form is,

$$G = 2\pi r D C. \tag{33}$$

The diffusivity measurements were generally made by releasing a tracer gas at a known rate, G, measuring the concentration, C, at a certain distance, r, from the source, and solving for D.

Equations 32 and 33 apply only to the special case of a constant generation rate. If G varies with time, the more fundamental expression found in Crank must be used instead:[35]

$$C = \frac{M}{8(\pi Dt)^{1.5}} \exp\left(\frac{-r^2}{4Dt}\right). \tag{34}$$

This is the equation for diffusion of a point source in an infinite volume, when a mass, M, is instantaneously introduced. Adaptation to hemispherical transport is as follows, with the concentration twice as large because the contaminant is constrained to filling half the volume:

$$C = \frac{M}{4(\pi Dt)^{1.5}} \exp\left(\frac{-r^2}{4Dt}\right), \tag{35}$$

M is a mass of contaminant instantaneously introduced at the center of the base of the hemisphere. Nicas approximated a known emission rate function as a series of masses, then calculated the time-varying concentration, using Equation 35.[1] Rearranging Equation 35 as follows,

$$M = 4(\pi Dt)^{1.5} C \exp\left(\frac{r^2}{4Dt}\right), \tag{36}$$

the current authors calculated a series of masses using an inductive, iterative process applied to the concentration data, then approximated G from the series of masses. However, this calculation was unstable and produced physically unrealistic results, oscillating between ever-growing positive and negative values for M and G. From inspecting Equations 35 and 36, it is clear that solving for M is inherently less stable than solving for C, because the equation for M involves exponential growth, whereas the equation for C involves exponential decay. A stable algorithm for calculating M and G is the subject of ongoing research, although application of the UD model to time-varying emission rates is not discussed further in this article.

TABLE I. Experimental Design

Variable	Model[A]			
	CM-1	CM-2	CM-L	UD
Source location	floor, pump, table	table	floor, pump, table	floor, pump, table
Source type	constant time-varying	constant time-varying	time-varying	constant time-varying
Receptor location[B]	A1, A2, BZ, CEA, EX	BZ	A1, A2, BZ, CEA, EX	A1, A2, BZ, CEA, EX
Ventilation rate (m^3/min)	0.522, 2.44, 6.23	0.522, 2.44, 6.23	0.522, 2.44, 6.23	0.522, 2.44, 6.23

[A]CM-1 and CM-2: one-zone and two-zone completely mixed models; CM-L: location-based time-dependent model; UD: uniform eddy diffusivity model
[B]A1 and A2: areas 1 and 2; BZ: breathing zone; CEA: inlet to CEA instrument (TGM-555 toxic gas monitor); EX: exhaust duct

Study Design

Once C(x,y,z,t) was obtained through CFD simulation, concentration information was available for thousands of locations in the room volume. Particular attention was paid to the monitoring locations where Stewart et al. collected data and to the exhaust duct. These represent the locations most likely to be chosen by an industrial hygienist for making actual concentration measurements. In evaluating the CM-1 model, concentration at the CEA inlet location was used. For the CM-2 model the BZ concentration was used as the near-field concentration, and the exhaust concentration as the far-field. The UD model employed the BZ concentration. For the time-dependent case the model emission estimates were compared with the emission used for CFD simulation, with respect to total mass and shape. Table I summarizes the study design. These comparisons were done at three ventilation rates to investigate the effects of this variable on the accuracy of emission estimates.

Calculation of Model Parameters

CM-1 does not require calculation of parameters. For the CM-2 model the near field was constructed as a hemisphere with radius equal to the distance between the center of the source cell and the center of the BZ cell.[6,8] The airspeed calculated in the CFD simulation for each cell was averaged over the upwind boundary of the hemisphere and multiplied by the projected area of the hemisphere to approximate the inter-zone exchange rate, β. To apply the UD model, the eddy diffusivity, D, was calculated from Equation 33 using the concentrations at A1, A2, BZ, and CEA resulting from the three source locations. Thus, D was calculated along 12 distinct paths in the room. The average of these values was interpreted as the isotropic eddy diffusivity for the room. This calculation was repeated at each ventilation rate.

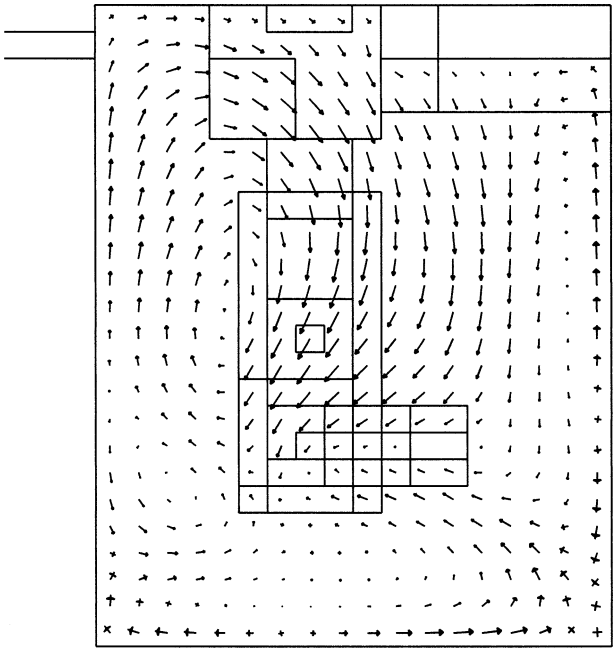

FIGURE 6. Velocity vectors at breathing zone height for the moderate ventilation rate

RESULTS

CFD Solutions

Steady-State

The simulated concentration fields at BZ height are shown graphically in Figures 2–4, for the floor, pump, and table source locations, respectively, at the moderate ventilation rate. In this isometric view of the room, contours of constant concentration are plotted for a horizontal plane 1.5 m above the floor. The contaminant source is the black square. These graphs show the range of concentration and the complexity of the pattern. Note that only for the table source was the highest breathing zone plane concentration directly above the source. For the floor source the maximum concentration in the breathing zone plane was closer to the exhaust than to the source. Thus, although the highest concentration must logically be at the source, and the simulations showed this in that the cell adjacent to the source always had the highest concentration, the conventional idea that concentration decreases in all directions with distance from source did not apply. It is tempting to then conclude that the region of maximum BZ plane concentration was drawn toward the exhaust, as with local exhaust ventilation. However, this did not occur for the pump source, which was closer to the exhaust than the floor source was. The maximum in that plane was between the worker and the source, rather than between the source and the exhaust. The value of CFD in computing the concentration field, when intuition fails to grasp the complexity of convective transport, is apparent.

Having seen how the concentration fields vary with location, it is natural to think about the mass transport processes in room air. Figure 6 shows the velocity vectors at BZ height for the moderate ventilation rate. The same pattern was observed for low and high ventilation rates. A clockwise circulation characterized the horizontal flow for most of the BZ plane. The contours for the floor and pump sources (Figures 2 and 3) show that this circulation maintained a relatively uniform concentration. For the floor source the concentration decreased gradually outside the circulation because the distance from the floor to the BZ plane allowed

TABLE II. CM-1 Emission Estimates for Steady-State Case

Flow Rate (m^3/min)	Receptor Location	Source Location	Emission Rate Estimate (mL $CH_2O_{(g)}$/min)	True Emission Rate (mL $CH_2O_{(g)}$/min)	Error (%)	Mean Absolute Value of Error (%)
0.522	A1	floor	15.2	16.3	−6.92	56.6
	A1	pump	23.7		45.2	
	A1	table	15.4		−5.32	
	A2	floor	20.5		25.7	
	A2	pump	14.7		−9.80	
	A2	table	19.3		18.4	
	BZ	floor	9.87		−39.6	
	BZ	pump	15.4		−5.32	
	BZ	table	75.7		364	
	CEA	floor	11.1		−32.2	
	CEA	pump	13.4		−18.1	
	CEA	table	34.0		109	
2.44	A1	floor	16.6	16.3	1.52	47.3
	A1	pump	23.0		41.0	
	A1	table	16.3		−0.13	
	A2	floor	20.7		26.8	
	A2	pump	15.5		−5.21	
	A2	table	19.8		21.2	
	BZ	floor	10.5		−35.4	
	BZ	pump	15.6		−4.46	
	BZ	table	62.0		279.8	
	CEA	floor	11.4		−30.3	
	CEA	pump	14.8		−9.10	
	CEA	table	34.6		112	
6.23	A1	floor	16.9	16.3	3.45	47.7
	A1	pump	22.4		37.0	
	A1	table	16.4		0.78	
	A2	floor	21.7		33.2	
	A2	pump	15.8		−3.42	
	A2	table	19.8		21.0	
	BZ	floor	10.6		−35.1	
	BZ	pump	15.1		−7.24	
	BZ	table	62.1		281	
	CEA	floor	11.5		−29.4	
	CEA	pump	14.6		−10.3	
	CEA	table	34.4		111	

mixing. The concentration for the pump source dropped off abruptly outside the circulation because the source was inside the circulation. Low magnitude velocity vectors converged into a small low-airspeed region above the table source and in front of the embalmer, coincident with the maximum concentration.

For the steady-state CM-1 and UD models the error ranged from −40.0 to +364.0% and from −44.7 to +89.0%, respectively, as shown in Tables II and III. Ventilation rate had very little effect on error. Location had a large impact. All models are compared in Table IV for a source located on the table and concentration measured at an appropriate location for each model. Thus, the concentration at the CEA instrument location was used for CM-1, because that is the location used for CM-1 by Bennett et al.[5,6] The BZ location was used for CM-2 because it is in the near-field.[8] BZ is used here for UD as a comparison with CM-2. For these scenarios UD agreed best with the CFD results, followed by CM-2, then CM-1. However, the CM-1 model improved for locations further from the source. The overall mean error was 34.6% for CM-1 and 10.8% for UD. The overall mean error absolute value was 50.5% for CM-1 and 29.8% for UD. CM-2 is not intended for these other combinations of source and monitoring location.

Time Dependent

The models were used in the fully time-dependent scenario, in which the time-varying concentration response to a time-varying emission rate was used to estimate what the emission rate function had been. The true emission rate and the simulated concentration at the BZ, CEA, and exhaust locations are shown in Figure 5.

Estimated emission rate as a function of time is shown in Figure 7 for CM-1, CM-2, and CM-L, compared with the actual emission rate function used as the CFD boundary condition. CM-1 overestimates at first, then underestimates becoming negative, which is physically unreasonable in this application. CM-2 overestimates during the entire emission period. CM-L has a shape somewhat similar to the true emission., but lags by about 30 sec. It is slightly negative in part of the tail.

When G(t) was integrated to obtain the total mass emitted, for the table source, CM-1 was more accurate than CM-2. CM-L was the most accurate, as shown in Table V. For CM-1 applied to all source and receptor locations, Table VI shows the time-dependent emission estimates. The error ranged from −40 to +426%, with emission estimates becoming slightly more accurate as ventilation rate increases. CM-L performed better than CM-1 for the other

TABLE III. UD Emission Estimates for Steady-State Case

Flow Rate (m^3/min)	Receptor Location	Source Location	Emission Rate Estimate (mL $CH_2O_{(g)}$/min)	True Emission Rate (mL $CH_2O_{(g)}$/min)	Error (%)	Mean Absolute Value of Error (%)
0.522	A1	floor	21.9	16.3	34.0	31.7
	A1	pump	21.9		34.4	
	A1	table	12.8		−21.6	
	A2	floor	30.0		83.7	
	A2	pump	11.7		−28.2	
	A2	table	16.8		3.14	
	BZ	floor	9.03		−44.7	
	BZ	pump	17.9		9.68	
	BZ	table	24.9		52.4	
	CEA	floor	12.4		−24.0	
	CEA	pump	19.0		16.6	
	CEA	table	20.8		27.6	
2.44	A1	floor	23.2	16.3	42.3	28.9
	A1	pump	20.7		27.1	
	A1	table	13.1		−19.5	
	A2	floor	29.4		80.4	
	A2	pump	12.0		−26.6	
	A2	table	16.8		2.90	
	BZ	floor	9.39		−42.5	
	BZ	pump	17.6		7.77	
	BZ	table	19.8		21.5	
	CEA	floor	12.4		−23.98	
	CEA	pump	20.6		26.0	
	CEA	table	20.6		26.5	
6.23	A1	floor	23.6	16.3	44.6	28.7
	A1	pump	20.1		23.2	
	A1	table	13.2		−19.0	
	A2	floor	30.8		89.0	
	A2	pump	12.2		−25.4	
	A2	table	16.7		2.39	
	BZ	floor	9.41		−42.4	
	BZ	pump	17.0		4.33	
	BZ	table	19.8		21.4	
	CEA	floor	12.5		−23.2	
	CEA	pump	20.2		24.0	
	CEA	table	20.5		25.4	

source receptor pairs, as shown in Table VII. Error ranged from −28.4 to +155.0%.

DISCUSSION

In steady-state conditions Table IV shows CM-1 at its near worst and CM-2 and UD at their best. However, the mean error absolute value in CM-1, for all source/receptor locations, is lower than CM-2 at its best and higher than UD at its best. The spatial pattern of error in CM-1 was found to be durable over a range of ventilation rates. The error due to location was nearly independent of ventilation rate, and ventilation rate (within the range studied) had little effect. This behavior allows the overall error to be approximated in terms of location, i, an idea developed in the Methods section and written explicitly as Equation 37, which defines an error function, f_E:

$$f_E(Q, i) \approx f_{Ei}(i) f_{EQ}(Q) \approx f_{Ei}(i) = \lambda_i - 1. \quad (37)$$

The first part of Equation 37 expresses that the errors in the steady-state CM-1 model due to location and due to ventilation rate are nearly independent. The second part shows that the error due to ventilation rate is negligible, and the third part relates the error function to the location factor.

The steady-state results for this work are somewhat different from those reported by Feigley et al.[36] There, CM-1, CM-2, and UD deviated from the CFD concentrations with mean errors of −21.9, 32.2, and 126.0%, respectively, in the source near-field and −4.80, −2.30, and −36.3% in the far-field. The standard deviations of the errors were 26.8, 111.0, and 103.0% in the near-field and 29.5, 31.4, 28.4% in the far-field. Ranking the models in terms of agreement with CFD put UD on the bottom, whereas in the present work, UD ranked at the top for the steady-state case. The CFD methods were identical except for a small difference in cell size. The departure from earlier results can be attributed to differences in the rooms. The simulated room in Feigley et al. was open, other than a 1-m^3 source table; whereas here the simulated room contained shelves, cabinets, table, worker, and equipment. Flows around these bluff bodies generated turbulence, which contributed to eddy diffusivity, the assumed contaminant dispersion mechanism of the UD model. Also, the forced convection pattern had some nearly room-scale circulations, which enhanced the rotational symmetry about the vertical axis of the concentration field, with respect to the source. This symmetry is characteristic of concentration fields produced by the UD model. It is worth noting that the maximum overestimations reported in Feigley et al. for the wall jet cases (mean=409%) were larger than

TABLE IV. Steady-State Generation Rate for Table Source

Q (m^3/min)	CFD G (mL/min)	CFD C_{CEA} (ppm)	CFD C_{BZ} (ppm)	CM-1 G CEA	UD G BZ	CM-2 G BZ	D (m^2/min)	Beta (m^3/min)
0.522	16.3	65.2	145	34.0	24.9	30.6	0.0450	0.353
2.44	16.3	14.2	25.4	34.6	19.8	26.5	0.205	1.82
6.23	16.3	5.53	9.97	34.4	19.8	27.0	0.521	4.78
Q					Error %			
0.522				109	52.4	87.2		
2.44				113	21.4	62.1		
6.23				111	21.4	65.2		

those for the ceiling diffuser cases (mean=249%). The present study used a ceiling diffuser only. Thus, the UD results for the previous study and for the present study agreed more closely when only the ceiling diffuser cases were considered, probably due to a similarity in the flow fields.

The form of a time-dependent emission rate function greatly affects the accuracy of each of these mass balance models. Performance is lowest when the hypothetical emission is much different in character from the intended application of the model. For example, Nicas[1] shows how the model proposed by Bennett et al.[5] mischaracterizes a constant emission rate, particularly at start-up. However, in Bennett et al. the authors state that their model is intended for an emission rate function with "distinct peaks," and that their predicted emission rate functions will therefore have a "rise and fall." In another instance Nicas shows that the model in Bennett et al. is inaccurate for an emission rate that decays exponentially, starting at time equal to zero. Again, the scope of the model's intended application is exceeded, because Nicas's example function had no "rise," only "fall." Statements about model accuracy acquire more meaning as the standard against which the model is compared becomes more accurate. In relating C and G for both of these illustrations of the CM-1 model, Nicas used the assumption of uniform eddy diffusivity. Complete mixing and uniform eddy diffusivity are both physical idealizations. Moreover,

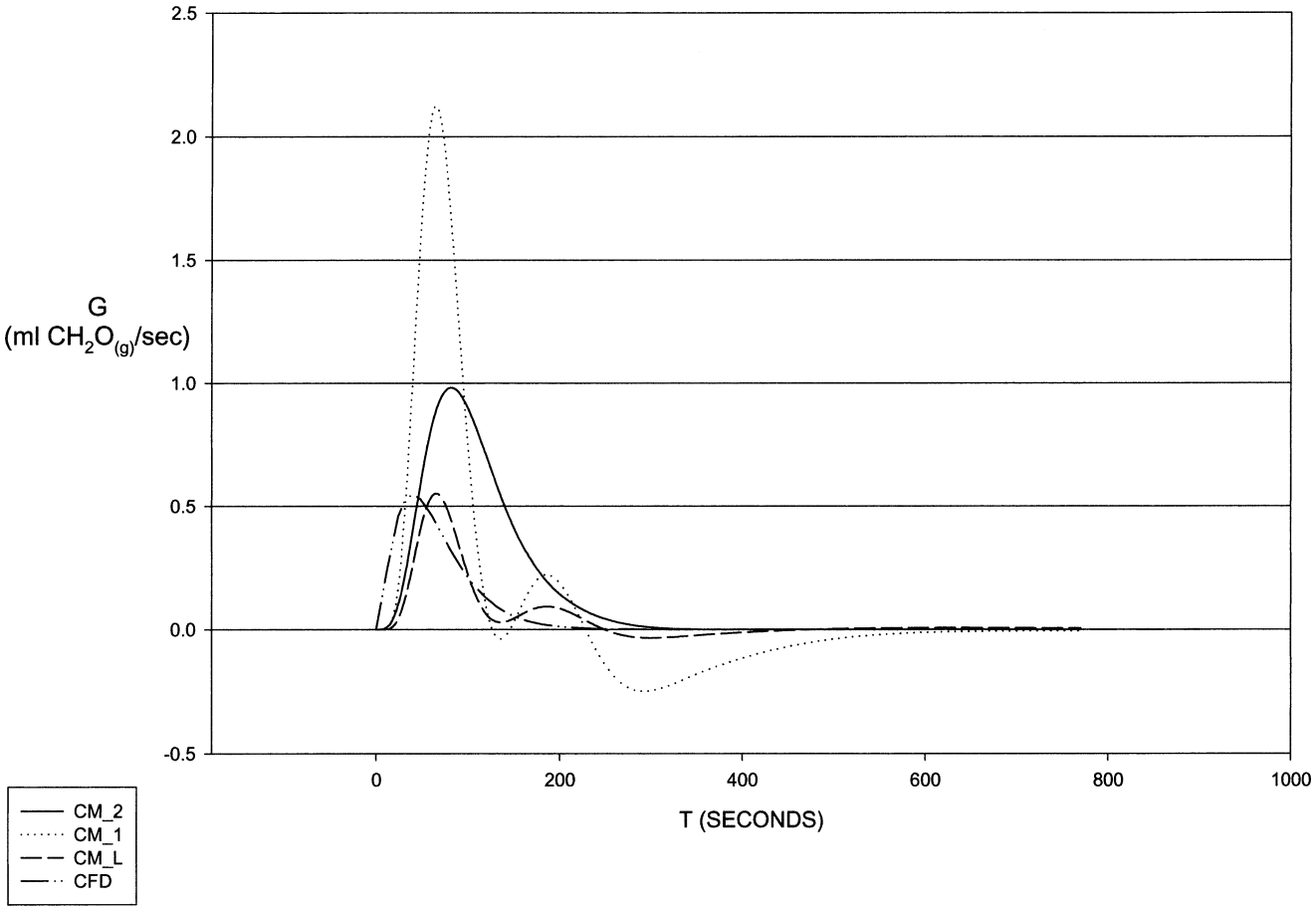

FIGURE 7. Estimated emission rate as a function of time for CM-1, CM-2, and CM-L, compared with the actual emission rate function used as the CFD boundary condition

TABLE V. Mass Generated by Time-Dependent Source on Table

Q (m^3/min)	CFD γ (mL $CH_2O_{(g)}$)	CM-1 γ CEA (mL $CH_2O_{(g)}$)	CM-L γ CEA (mL $CH_2O_{(g)}$)	CM2 γ BZ (mL $CH_2O_{(g)}$)	D (m^2/min)	Beta (m^3/min)
0.522	45.5	104	40.6	107	0.0450	0.353
2.44		97.3	36.5	106	0.205	1.82
6.23		90.9	33.9	125	0.521	4.78
Q			Error %			
0.522		129	−10.7	135		
2.44		114	−19.8	133		
6.23		99.8	−32.9	175		

TABLE VI. CM-1 Emission Estimates for Time-Dependent Case

Flow Rate (m^3/min)	Receptor Location	Source Location	Emission Estimate (mL $CH_2O_{(g)}$)	Emission Estimate (mg $CH_2O_{(g)}$)	True Emission (mL $CH_2O_{(g)}$)	Error (%)	Mean Absolute Value of Error (%)
0.522	A1	floor	41.5	51.4	45.5	−8.50	52.2
	A1	pump	65.2	80.7		43.7	
	A1	table	241.8	51.8		−7.84	
	A2	floor	59.4	73.5		30.7	
	A2	pump	40.6	50.3		−10.6	
	A2	table	53.2	65.9		17.2	
	BZ	floor	27.2	33.7		−40.1	
	BZ	pump	41.1	50.8		−9.56	
	BZ	table	239	296		426	
	CEA	floor	32.2	39.8		−29.2	
	CEA	pump	35.8	44.3		−21.1	
	CEA	table	104	129		129	
	EX	floor	44.8	55.5		−1.32	
	EX	pump	44.0	54.5		−3.08	
	EX	table	43.5	53.9		−4.19	
2.44	A1	floor	46.1	57.1	45.5	1.61	42.7
	A1	pump	63.3	78.3		39.3	
	A1	table	44.9	55.6		−1.12	
	A2	floor	59.5	73.7		31.2	
	A2	pump	42.8	53.0		−5.73	
	A2	table	54.6	67.6		20.2	
	BZ	floor	28.9	35.8		−36.3	
	BZ	pump	42.0	52.0		−7.49	
	BZ	table	197	244		334	
	CEA	floor	31.6	39.1		−30.4	
	CEA	pump	40.4	50.0		−11.1	
	CEA	table	97.3	120.5		114	
	EX	floor	46.5	57.6		2.42	
	EX	pump	46.5	57.6		2.42	
	EX	table	46.4	57.4		2.20	
6.23	A1	floor	46.0	56.9	45.5	1.23	39.3
	A1	pump	61.0	75.5		34.3	
	A1	table	44.5	55.1		−1.89	
	A2	floor	59.1	73.1		30.1	
	A2	pump	42.9	53.1		−5.59	
	A2	table	54.4	67.3		19.8	
	BZ	floor	28.7	35.5		−36.8	
	BZ	pump	41.3	51.1		−9.03	
	BZ	table	185	229		307	
	CEA	floor	31.3	38.7		−31.1	
	CEA	pump	39.9	49.4		−12.0	
	CEA	table	90.9	113		100.3	
	EX	floor	45.4	56.2		0.00	
	EX	pump	45.4	56.2		0.00	
	EX	table	45.3	56.1		−0.220	

TABLE VII. CM-L Emission Estimates for Time-Dependent Case

Flow Rate (m^3/min)	Receptor Location	Source Location	Emission Estimate (mL $CH_2O_{(g)}$)	Emission Estimate (mg $CH_2O_{(g)}$)	True Emission (mL $CH_2O_{(g)}$)	Error (%)	Mean Absolute Value of Error (%)
0.522	A1	floor	46.4	57.4	45.5	1.98	9.23
	A1	pump	46.0	56.9		1.10	
	A1	table	38.0	47.0		−16.5	
	A2	floor	48.4	59.9		6.37	
	A2	pump	37.2	46.1		−18.2	
	A2	table	42.8	53.0		−5.93	
	BZ	floor	35.3	43.7		−22.4	
	BZ	pump	46.3	57.3		1.76	
	BZ	table	41.0	50.8		−9.89	
	CEA	floor	40.9	50.6		−10.1	
	CEA	pump	42.9	53.1		−5.71	
	CEA	table	40.6	50.3		−10.8	
2.44	A1	floor	47.2	58.4	45.5	3.74	36.6
	A1	pump	31.1	38.5		−31.6	
	A1	table	37.1	45.9		−18.5	
	A2	floor	50.4	62.4		10.8	
	A2	pump	116	144		155	
	A2	table	42.8	53.0		−5.93	
	BZ	floor	33.8	41.8		−25.7	
	BZ	pump	84.6	105		85.9	
	BZ	table	45.4	56.2		−0.220	
	CEA	floor	40.2	49.8		−11.6	
	CEA	pump	75.8	93.8		66.6	
	CEA	table	34.7	43.0		−23.7	
6.23	A1	floor	47.5	58.8	45.5	4.40	13.3
	A1	pump	45.0	55.7		−1.10	
	A1	table	35.0	43.3		−23.1	
	A2	floor	50.0	61.9		9.89	
	A2	pump	34.4	42.6		−24.4	
	A2	table	42.3	52.4		−7.03	
	BZ	floor	31.7	39.2		−30.3	
	BZ	pump	45.7	56.6		0.440	
	BZ	table	49.9	61.8		9.67	
	CEA	floor	38.9	48.2		−14.5	
	CEA	pump	42.4	52.5		−6.81	
	CEA	table	32.6	40.4		−28.4	

these assumptions differ diametrically. It would be no less valid to assume a spatially uniform concentration and proceed to show the inaccuracy of the UD model in that context.

Returning to the present study, the total emission for the time-dependent source was most accurately represented by CM-L. CM-1 overestimated, and CM-2 overestimated more. If only the total emission is important, then the best approach is to integrate Equation 4, with respect to time (as in Equation 7), using the time-dependent concentration measured in the exhaust duct.

Table VI shows that CM-1 emission estimates were slightly more accurate for high than for low ventilation, indicating a faster flattening of the concentration gradient due to a higher rate of transport away from the point source. In contrast the embalming experiments in Bennett et al. showed more spatial uniformity in the time-weighted averages under low ventilation.[5] Here, the departure from the earlier result is explained by the current study enlisting a single emission event, whereas in Bennett et al. a sequence of emission events occurred. There, emissions that occurred early in the embalmings contributed to the full-period average in a well-mixed manner for a large portion of the averaging time, especially for the low ventilation condition because the residence time was longer.

As in the steady-state case, receptor and source location were by far the most important variables in determining emission model accuracy. Table VII indicates that the CM-L model achieves reasonably good accuracy by making use of the steady-state location effect, applying it to the time-dependent case. The largest departures from the CFD generation rate occurred for the pump source, because the room maintained an unmixed state beyond the integration period of 15 min. Some of the predicted generation rate (in some cases slightly negative in the tail) was not included in the total mass prediction because of truncation.

CONCLUSIONS AND RECOMMENDATIONS

The simple deterministic models evaluated in this study work well or poorly depending on their application, even when the application is limited to a point source in a room under general ventilation. The authors used agreement with the results of CFD simulations as a basis of comparison with four simple deterministic models. However, no finite group of simulations, experiments, or field studies will fully represent the universe of possible scenarios to which these models may be reasonably applied by industrial hygienists. This is a limitation shared by any method of model evaluation.

For the steady-state case the UD model estimates were closest to the CFD simulation results. When the source near-field contained the breathing zone receptor, the CM-2 model was applied. Then, in decreasing agreement with CFD were UD, CM-2, and CM-1. Averaging over all source and receptor locations (CM-2 applied for only one), in decreasing order of agreement with CFD were UD, CM-1, and CM-2. Source and receptor location had a large effect on emission estimates using the CM-1 model and some effect using the UD model. A location-specific mixing factor (location factor) can be used confidently with CM-1 across a range of ventilation rates. With the error in CM-1 limited to the location effect, the model can be useful under a variety of conditions, if location is held constant or if an accurate location factor is applied.

For the time-dependent case the easily found steady-state location factor can be used to build a more accurate emission model, CM-L, that can be applied to any source/receptor combination. Total mass emitted was modeled most accurately by CM-L, followed by CM-1 and CM-2, in decreasing order. Although UD was highly accurate for the steady-state, constant source scenario, it proved impractical for a time-dependent source, because the calculation was unstable, although ongoing research may reveal a more stable algorithm for this model. For the time-dependent embalming scenarios in Bennett et al.,[5] these findings suggest that CM-1 was a better choice than CM-2 or UD would have been, if they had been used.

Results for other rooms and conditions could be quite different, and the limited number (five, including the exhaust) of receptor locations used here did not fully characterize this particular room and set of conditions. The following recommendations for model application are offered cautiously.

(1) CM-1, CM-2, and UD should not be used to derive a generation rate from near-field concentration measurements when the airflow near a source has a well-defined direction, with the exception that CM-1 may be used upwind or with a location factor for the steady-state case, λ. Although not investigated in this article, the UD model modified to include advection may be a good candidate for use downwind of a source. A weakness of all three of these models (other than CM-1 with λ and UD with advection) is their assumption of concentration symmetry with respect to a point source, because a plume of higher concentration forms downwind to the extent that the flow is directional. However, in real rooms, worker movement, breathing, and natural convection due to heat sources create more random flow elements that are superimposed on the mean airflow patterns created by forced convection. It is likely that the accuracy of CM-1, CM-2, and UD are enhanced by these factors associated with real room airflows.

(2) CFD models using coarse grids and RANS turbulence models can provide good information on airflows where the forced convection from air inlets dominates, compared with the disorganized flows mentioned previously. Thus, for the situations where CM-1, CM-2, and UD are weak, CFD is an effective tool for understanding the behavior of these models. Conversely, the application of CFD to flows highly influenced by worker movement, breathing, and natural convection due to heat sources is difficult in terms of setting boundary conditions, finding sufficient computing resources, and obtaining convergence.

(3) Time-varying generation rate: CM-2 can be used effectively when the generation rate is being derived from near-field concentrations, keeping in mind recommendation (1). UD seems to not be stable. CM-1 is simple and robust but is less accurate than CM-L. CM-L is versatile because, unlike the other three models, it does not rely on the assumption of a particular room concentration structure. It is recommended that modelers consider using CM-L for time-varying generation rate estimation in workrooms under general ventilation, so that its accuracy may be investigated further.

The CFD simulations in this study all started with a contaminant emission rate as a boundary condition and calculated a concentration field. This procedure is called the "forward" problem. The determination of location and emission rate of a contaminant source, known as source localization and source inversion, based on measured concentrations, is not currently within the capabilities of standard CFD simulations. It is known as the "inverse" problem, a current research area.[37] Another avenue that should be explored is the selection of a turbulence model that works well for airflows typical of occupied spaces. An impediment there (that is disappearing) is the difficulty in finding the necessary computing resources to simulate three-dimensional, time-dependent flows, with sufficient spatial and temporal resolution to resolve large eddies.

REFERENCES

1. **Nicas, M.:** The effect of concentration gradients on deducing a contaminant generation rate function. *Am. Ind. Hyg. Assoc. J. 59*:680–688 (1998).
2. **Wilcox, D.C.:** *Turbulence Modeling for CFD.* La Cañada, Calif.:: DCW Industries, 2000.
3. **Rota, R., G. Nano, and L. Canossa:** Design guidelines for push-pull ventilation systems through computational fluid dynamics modeling. *Am. Ind. Hyg. Assoc. J. 62*:141–148 (2001).
4. **Shibata, N., M. Tanaka, J. Ojima, and T. Iwasaki:** Numerical simulations to determine the most appropriate welding and ventilation conditions in small enclosed workspace. *Ind. Health 38*:356–365 (2000).
5. **Bennett, J.S., C.E. Feigley, D.W. Underhill, et al.:** Estimating the contribution of individual work tasks to room concentration: method applied to embalming. *Am. Ind. Hyg. Assoc. J. 57*:599–609 (1996).
6. **Bennett, J.S., C.E. Feigley, J. Khan, and H. Hosni:** Comparison of mathematical models for exposure assessment with computational fluid dynamic simulation. *Appl. Occup. Environ. Hyg. 15*:131–144 (2000).
7. **Nicas, M.:** Estimating exposure intensity in an imperfectly mixed room. *Am. Ind. Hyg. Assoc. J. 57*:542–550 (1996).
8. **Nicas, M., and S.L. Miller:** A multi-zone model evaluation of the efficacy of upper-room air ultraviolet germicidal irradiation. *Appl. Occup. Environ. Hyg. 14*:317–328 (1999).
9. **American Conference of Governmental Industrial Hygienists (ACGIH):** *Industrial Ventilation: A Manual of Recommended Practice,* 22nd ed. Cincinnati, Ohio: ACGIH, 1995.
10. **Scheff, P.A., R.L. Friedman, J.E. Franke, L.M. Conroy, and R.A. Wadden:** Source activity modeling of Freon emissions from open-top vapor degreasers. *Appl. Occup. Environ. Hyg. 7*:127–134 (1992).
11. **Wadden, R.A., P.A. Scheff, and J.E. Franke:** Emission factors for trichloroethylene vapor degreasers. *Am. Ind. Hyg. Assoc. J. 50*:496–500 (1989).
12. **Conroy, L.M., R.A. Wadden, P.A. Scheff, J.E. Franke, and C.B. Keil:** Workplace emission factors for hexavalent chromium plating. *Appl. Occup. Environ. Hyg. 10*:620–627 (1995).
13. **Keil, C.B., R.A. Wadden, P.A. Scheff, J.E. Franke, and L.M. Conroy:** Determination of multiple source volatile organic compound emission factors in offset printing shops. *Appl. Occup. Environ. Hyg. 12*:111–121 (1997).
14. **Stewart, P.A., R.F. Herrick, C.E. Feigley, et al.:** Study design for assessing exposures of embalmers for a case-control study: Part I. Monitoring results. *Appl. Occup. Environ. Hyg. 7*:532–540 (1992).
15. **Fluent, Inc.:** *Fluent 4.4 User's Guide*, vol. 4. Lebanon, N.H.: Fluent, Inc., 1997.
16. **Patankar, S.V.:** *Numerical Heat Transfer and Fluid Flow.* New York: Hemisphere, 1980.

17. **Awbi, H.B.:** *Ventilation of Buildings.* London: E & FN Spon, 1991.
18. **Fluent, Inc.:** *Fluent 4.4 User's Guide,* vol. 3. Lebanon, N.H.: Fluent, Inc., 1997.
19. **Patankar, S.V.:** *Numerical Heat Transfer and Fluid Flow.* New York: Hemisphere, 1980.
20. **Launder, B.E., and D.B. Spalding:** *Lectures in Mathematical Models of Turbulence.* London: Academic Press, 1972.
21. **Fluent, Inc.:** *Fluent 4.4 User's Guide,* vol. 1. Lebanon, N.H.: Fluent, Inc., 1997.
22. **Nielsen, P.V.:** *The Prescribed Velocity Method—A Practical Procedure for Introduction of an Air Terminal Device in CFD Calculation.* Aalborg, Denmark: Aalborg University, 1998.
23. **Nielsen, P.V.:** *The Box Method—A Practical Procedure for Introduction of an Air Terminal Device in CFD Calculation.* Aalborg, Denmark: Aalborg University, 1997.
24. **Zhang, J.S., L.L. Christianson, G.J. Wu, and R.H. Zhang:** Experimental evaluation of a numerical simulation model for predicting room air motion. *Indoor Environ. 2*:331–336 (1993).
25. **Bennett, J.S.:** "Exposure, Emission, and Control: Evaluation of the Completely-Mixed Mass Balance Model Using Computational Fluid Dynamics." Ph.D. diss., School of Public Health, University of South Carolina, Columbia, SC, 1999.
26. **Hinze, J.O.:** *Turbulence.* New York, McGraw-Hill, 1975.
27. **Sandia National Laboratories:** *Verification and Validation in Computational Fluid Dynamics* by W.L. Oberkampf and T.G. Trucano (SAND2002–0529). Springfield, Va.: U.S. Department of Commerce/National Technical Information Service, 2002.
28. **Hosni, M.H., K. Tsai, and A.N. Hawkins:** Numerical predictions of room air motion. In *American Society of Mechanical Engineers (ASME) Fluids Engineering Division Conference Proceedings,* vol. 2. Fairfield, N.J.: ASME, 1996.
29. **Baker, A.J., M.B. Taylor, N.S. Winowich, and M.R. Heller:** Prediction of the distribution of indoor air quality and comfort in aircraft cabins using computational fluid dynamics (CFD). In *Air Quality and Comfort in Airliner Cabins.* West Conshohocken, Pa.: American Society for Testing and Materials, 2000.
30. **Oberkampf, W.L., and T.G. Trucano:** Validation methodology in computational fluid dynamics. In *Fluids 2000,* Proceedings of Fluids 2000 Conference, Denver, Colo., June 19–22, 2000, p. 9, AIAA 2000–2549. Reston, Va.: American Institute of Aeronautics and Astronautics (AIAA).
31. **Cheney, W., and D. Kincaid:** *Numerical Mathematics and Computing.* Monterey, Calif.: Brooks/Cole, 1980.
32. **Koffman, E.B., and F.L. Friedman:** *FORTRAN with Engineering Applications.* Reading, Pa.: Addison-Wesley, 1993.
33. **Senior, T.B.A.:** *Mathematical Methods in Electrical Engineering.* Cambridge, U.K.: Cambridge University Press, 1986.
34. **Tennekes, H., and J.L. Lumley:** *A First Course in Turbulence.* Cambridge, Mass.: MIT Press, 1972.
35. **Crank, J.:** *Mathematics of Diffusion.* Oxford, U.K.: Clarendon Press, 1975.
36. **Feigley, C.E., J.S. Bennett, J. Khan, and E. Lee:** Performance of deterministic workplace exposure assessment models for various contaminant source, air inlet, and exhaust locations. *Am. Ind. Hyg. Assoc. J. 63*:402–412 (2002).
37. **Smith, T.M., G. Hennigan, R. Pawlowski, et al.:** "Large-scale transport/reaction simulations: Turbulent pool Fire Simulations, Semiconductor Materials Processing Calculations and Chem-Bio Threat Analysis using MPSalsa on CPlant" (Technical report). Livermore, Calif.: Sandia National Laboratories. [In progress]
38. **Wilcox, D.C.:** *Turbulence Modeling for CFD.* La Cañada, Calif.: DCW Industries, 2000.
39. **Anderson, D.A., J.C. Tannehill, and R.H. Pletcher:** *Computational Fluid Dynamics and Heat Transfer.* New York: Hemisphere, 1984.
40. **Hinze, J.O.:** *Turbulence.* New York, McGraw-Hill, 1975.
41. **Wilcox, D.C.:** *Turbulence Modeling for CFD.* La Cañada, Calif.: DCW Industries, 2000.

APPENDIX

Turbulence Modeling

The k-ϵ turbulence model invokes the Boussinesq hypothesis, to help provide closure for the RANS equations.[17,38,39] Reynolds averaging decomposes the velocity components of a stationary flow into a constant average and a random fluctuation, that is,

$$u(t) = U + u'(t) \quad (38)$$

$$v(t) = V + v'(t) \quad (39)$$

$$w(t) = W + w'(t), \quad (40)$$

where the capitol indicates the average and the prime indicates the fluctuation.[26,38,39] When the conservation of momentum equations (for illustration we look now only at the x-direction) are written in terms of Reynolds averages, terms arise involving the product of fluctuations:

$$\frac{\partial}{\partial t}(\rho u) + \frac{\partial}{\partial x}(\rho uu) + \frac{\partial}{\partial y}(\rho vu) + \frac{\partial}{\partial z}(\rho wu) = \frac{\partial}{\partial x}\left(\Gamma_u \frac{\partial u}{\partial x}\right) + \frac{\partial}{\partial y}\left(\Gamma_u \frac{\partial u}{\partial y}\right) + \frac{\partial}{\partial z}\left(\Gamma_u \frac{\partial u}{\partial z}\right) + S_u. \quad (41)$$

The left side of the equation becomes:

$$\frac{\partial}{\partial t}[\rho(U + u')] + \frac{\partial}{\partial x}[\rho(U^2 + 2Uu' + u'^2)] + \frac{\partial}{\partial y}[\rho(VU + Vu' + Uv' + u'v')] + \frac{\partial}{\partial z}[\rho(WU + Wu' + Uw' + u'w')]. \quad (42)$$

Now, the mean of a fluctuation or a product of a mean and a fluctuation is zero, for example,

$$\overline{u'} = 0 \quad \text{and} \quad \overline{u'V} = 0, \quad (43)$$

where the overbar indicates the mean.[26]Then, taking the overall mean results in:

$$\frac{\partial}{\partial t}(\rho U) + \frac{\partial}{\partial x}[\rho(U^2 + \overline{u'^2})] + \frac{\partial}{\partial y}[\rho(VU + \overline{u'v'})] + \frac{\partial}{\partial z}[\rho(WU + \overline{u'w'})] \quad (44)$$

which can be rearranged as:

$$\frac{\partial}{\partial t}(\rho U) + \frac{\partial}{\partial x}(\rho U^2) + \frac{\partial}{\partial y}(\rho VU) + \frac{\partial}{\partial z}(\rho WU) - \frac{\partial}{\partial x}\overline{u'^2} - \frac{\partial}{\partial y}\rho\overline{u'w'} - \frac{\partial}{\partial z}\rho\overline{u'v'}. \quad (45)$$

The terms $-\rho\overline{u'^2}$, $-\rho\overline{u'v'}$, and $-\rho\overline{u'w'}$ are *Reynolds stresses.*[17,38,40] The momentum equations in the y- and z-directions also each contribute three Reynolds stresses for a total of nine. Six of these are independent. Thus, six unknowns have been added to the system of equations that govern three-dimensional fluid motion. These terms create the closure problem when trying to solve turbulent flows using mean flow quantities. Boussinesq defined a *turbulent viscosity,* μ_T, and put forth the idea that the Reynolds stresses can be calculated from this turbulent viscosity and the mean flow quantities.[38,40] Launder and Spalding formulated an equation for the eddy viscosity:[20]

$$\mu_T = \rho C_\mu \frac{k^2}{\varepsilon}. \quad (46)$$

The turbulent kinetic energy, k, and the dissipation rate, ϵ, were determined simultaneously in a system of two transport equations with the form of Equation 1:[21,17]

$$\frac{\partial}{\partial t}(\rho k) + \frac{\partial}{\partial x}(\rho u k) + \frac{\partial}{\partial y}(\rho v k) + \frac{\partial}{\partial z}(\rho w k) = \frac{\partial}{\partial x}\left(\Gamma_k \frac{\partial k}{\partial x}\right) + \frac{\partial}{\partial y}\left(\Gamma_k \frac{\partial k}{\partial y}\right) + \frac{\partial}{\partial z}\left(\Gamma_k \frac{\partial k}{\partial z}\right) + S_k \quad (47)$$

$$\frac{\partial}{\partial t}(\rho \varepsilon) + \frac{\partial}{\partial x}(\rho u \varepsilon) + \frac{\partial}{\partial y}(\rho v \varepsilon) + \frac{\partial}{\partial z}(\rho w \varepsilon) = \frac{\partial}{\partial x}\left(\Gamma_\varepsilon \frac{\partial \varepsilon}{\partial x}\right) + \frac{\partial}{\partial y}\left(\Gamma_\varepsilon \frac{\partial \varepsilon}{\partial y}\right) + \frac{\partial}{\partial z}\left(\Gamma_\varepsilon \frac{\partial \varepsilon}{\partial z}\right) + S_\varepsilon \quad (48)$$

where

$$\Gamma_k = \frac{\mu + \mu_T}{\sigma_k}, \quad (49)$$

$$\Gamma_\varepsilon = \frac{\mu + \mu_T}{\sigma_\varepsilon}, \quad (50)$$

$$S_k = G_S - \rho\varepsilon, \quad \text{and} \quad (51)$$

$$S_\varepsilon = C_1 \frac{\varepsilon}{k} G_S - C_2 \rho \frac{\varepsilon^2}{k}. \quad (52)$$

The constants σ_k, σ_ϵ, C_1, C_2, and C_μ were empirically determined by Launder and Spalding through extensive experimentation on free turbulent flow. The values are 1.0, 1.3, 1.44, 1.92, and 0.09, respectively.[41] Like the standard k-ϵ model, these values are the default settings in the commercial CFD code.[21] G_S is the kinetic energy generated by shear stress and can be expressed in terms of the turbulent viscosity:[17]

$$G_S = \mu_T \left\{ 2\left[\left(\frac{\partial u}{\partial x}\right)^2 + \left(\frac{\partial v}{\partial y}\right)^2 + \left(\frac{\partial w}{\partial z}\right)^2\right] + \left(\frac{\partial u}{\partial y} + \frac{\partial v}{\partial x}\right)^2 + \left(\frac{\partial u}{\partial z} + \frac{\partial w}{\partial x}\right)^2 + \left(\frac{\partial v}{\partial z} + \frac{\partial w}{\partial y}\right)^2 \right\}. \quad (53)$$

This formulation does not include buoyancy effects, which is appropriate since the flow in the present study was assumed to be isothermal. The flow was assumed to be incompressible.

Near walls the k-ϵ model needs modification, because it was formulated for free turbulent flows.[7,21] With a cell size of 15.4 to 17.1 cm, the first layer of cells along a surface contained the viscous sublayer, and the distance from the surface to the first grid point fell within the log-law region, or occasionally within the blending region. The commercial CFD code handled the near-wall region according to the calculated value of the wall unit, y^*, a dimensionless distance that indicates position relative to the structure of the boundary layer.[21]